Chapter 7

CQD-Based Composites as Visible-Light Active Photocatalysts for Purification of Water

Abdullahi Baba Makama, Muneer Umar and Shettima Abdulkadir Saidu

Additional information is available at the end of the chapter

http://dx.doi.org/10.5772/intechopen.74245

Abstract

The unique physicochemical properties of carbon quantum dot-(CQD)-based photocatalysts, notably their exceptionally good light absorption in the UV and near-visible region, tunable photoluminescence, extraordinary upconversion photoluminescence, outstanding electron affinity, and photoinduced electron transfer, and electron mobility, have attracted considerable attention in different photocatalytic applications. In this review, we summarized the fundamental mechanism and thermodynamics of heterogeneous photocatalysis of aqueous pollutants and the fundamental multifaceted roles of CQDs in photoredox process. Furthermore, we discussed the recent developments in the use of CQD-based materials as visible-light active photocatalysts in water purification. Finally, the challenges and future direction of CQD-based materials as photocatalytic materials for environmental decontamination were highlighted.

Keywords: carbon, CQDs, photocatalyst, upconversion, visible-light

1. Introduction

Carbon quantum dots (CQDs) are a recently discovered class of carbon-based nanomaterials that are typically discrete, quasi-spherical, and less than 10 nm in size [1] (although CQDs of sizes >10 nm have been reported [2–5]). They are composed of sp^2/sp^3-hybridized carbon atoms, have various surface functional groups, and possess composition-dependent fluorescence. This relatively new material has attracted huge interest in many fields including, but not limited to, electrocatalysis [6], biosensing [7–10], bioimaging [11–14], chemical sensing [15],

and nanomedicine [16], due to their unique tunable photoluminescence (PL) properties, chemical inertness, high water solubility, ease and low cost of fabrication and, more importantly, low toxicity. Additionally, CQDs have also attracted considerable interest in various photocatalytic applications—environmental remediation [17–21], water splitting to produce H_2 production [22–27], CO_2 conversion [28–30], and synthesis of chemicals [28–33]—because when coupled with a semiconductor photocatalyst, CQDs can provide with several advantages, including improved light harvesting ability, efficient usage of the full spectrum of sunlight, efficient charge carrier separation, stability, and hinder charge recombination. **Figure 1** illustrates the various applications of CQDs in photocatalysis (left) and their competitive optical and structural properties during each photocatalytic procedure (right).

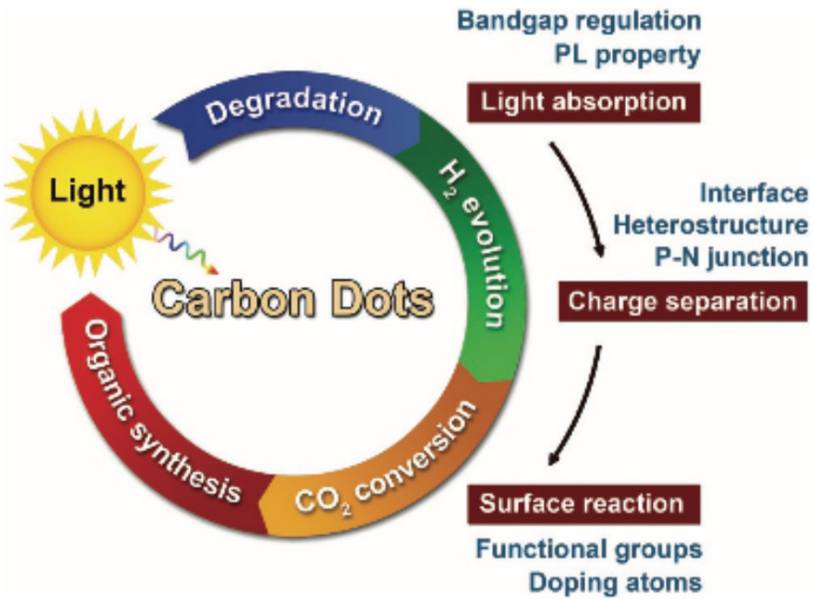

Figure 1. Illustration showing the different areas of applications of CQDs (reproduced from [34]).

2. Principles of heterogeneous photocatalysis

The fundamentals of heterogeneous photocatalysis underlying the degradation of a pollutant employing a semiconductor catalyst have been intensively reported in many literatures [35–41].

A semiconductor (SC) is a material that has a valence band (VB) and a nearly empty conduction band (CB) that are separated from one another by a band gap (E_g). In the ground state (i.e., at $T = 0\ K$), all the electrons are found in the VB of the SC. When illuminated by light of energy greater than or equal to the band gap ($h\nu \geq E_g$) of a semiconductor, electrons in the VB are excited to the CB, leaving behind equal number of voids (or holes) in the valence band. The generation of electron-hole pairs (e^-_{cb}/h^+_{vb}) is the first step in the heterogeneous photocatalysis of organic and inorganic compounds by semiconductors. This step is illustrated by the enlarged section of **Figure 2**. Once generated, the fate of the electron and hole can follow several de-excitation pathways as shown in **Figure 2**.

http://dx.doi.org/10.5772/intechopen.74245

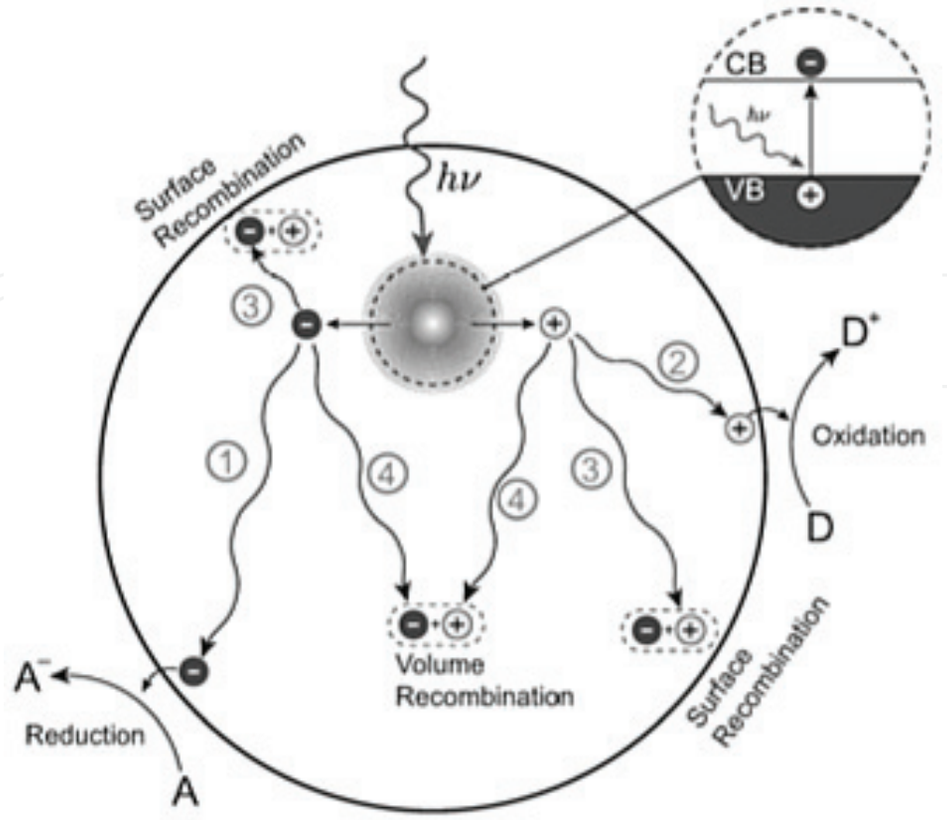

Figure 2. Schematic illustration of the principles and fundamental kinetic requirements of heterogeneous photocatalysis (reproduced from [43]).

First, the spatially separated charge carriers $\left(e_{cb}^{-}/h_{vb}^{+}\right)$ can migrate to the semiconductor surface where they can induce a redox reaction. At the surface, the electrons can be transferred to reduce an electron acceptor (A) (pathway **1**). On the other hand, a donor species (D) can donate an electron to the surface hole and gets oxidized in the process (pathway **2**). The probability and rate of the charge transfer processes for electrons and holes depends upon the respective positions of the band edges for the conduction and valence bands and the redox potential levels of the adsorbate species [40–42].

In competition with charge transfer to adsorbed species is electron and hole recombination. Recombination of the separated electron and hole can occur on the surface (pathway **3**) or in the volume of the semiconductor particle (pathway **4**). The electron-hole recombination can occur nonradioactively or radioactively to dissipate the input energy either as heat (E) or as a photon ($h\eta$) [44, 45], respectively. The widely postulated steps of heterogeneous photocatalysts may be summarized in a simplified way according to Eqs. (1)–(5).

$$\text{Charge generation}: \quad \text{SC} + h\eta\left(\geq E_g\right) \rightarrow \text{SC}\left(e^{-}/h^{+}\right) \tag{1}$$

$$\text{Charge separation}: \quad \text{SC}\left(e^{-}/h^{+}\right) \rightarrow \text{SC}\left(e_{cb}^{-}, h_{vb}^{+}\right) \tag{2}$$

$$\text{Charge recombination}: \quad \text{SC}\left(e_{vb}^{-}, h_{cb}^{+}\right) \rightarrow \text{SC} + \text{E or } h\eta \tag{3}$$

$$\text{Charge trapping}: \quad \mathrm{SC}\left(\mathrm{e}_{\mathrm{vb}}^{-}, \mathrm{h}_{\mathrm{cb}}^{+}\right) + 2\mathrm{Tr} \rightarrow \mathrm{SC}\left(\mathrm{e}_{\mathrm{Tr}}^{-}, \mathrm{h}_{\mathrm{Tr}}^{+}\right) \tag{4}$$

$$\text{Reduction reaction} \quad \mathrm{A} + \mathrm{e}_{\mathrm{Tr}}^{-} \rightarrow \mathrm{A}^{\bullet -} \tag{5}$$

$$\text{Oxidation reaction} \quad \mathrm{D} + \mathrm{h}_{\mathrm{Tr}}^{+} \rightarrow \mathrm{D}^{\bullet +} \tag{6}$$

A thermodynamic requirement of spontaneous reaction is a negative change in Gibb's energy, (i.e., $\Delta G < 0$) [46]. In a photocatalytic reaction, this condition is met when the quasi-Fermi (usually taken as the flat band potentials) energy levels of the photogenerated electrons and holes of the photocatalyst straddle the reduction/oxidation potentials of the substrate. In other words, the bottom of the photocatalyst's conduction bands (E_{CB}^{min}) must be located at a more negative potential than the reduction potential (E_{red}^{0}) of the substrate, while the top of its valence bands (E_{VB}^{max}) must be positioned more positively than the oxidation potential (E_{ox}^{0}) of the substrate [43, 47] as illustrated in **Figure 3**. Therefore, the spontaneity or otherwise the charge carrier-induced redox reactions, generically depicted by Eq. (5), is determined by the potential of the band edges of the semiconductor photocatalyst [48, 49].

As shown in **Figure 4**, the redox potential of the VB and the CB for different semiconductors varies between +4.0 and −1.5 V vs. normal hydrogen electrode (NHE), respectively. Many organic compounds have more negative oxidation potentials than the valence potential of most semiconductor photocatalysts. Accordingly, it is thermodynamically possible for the organic pollutants to be oxidized by photocatalysts. In contrast, fewer organic compounds can be reduced by photocatalyst since only a smaller number of them have a potential below that of the conduction band of most photocatalysts [50].

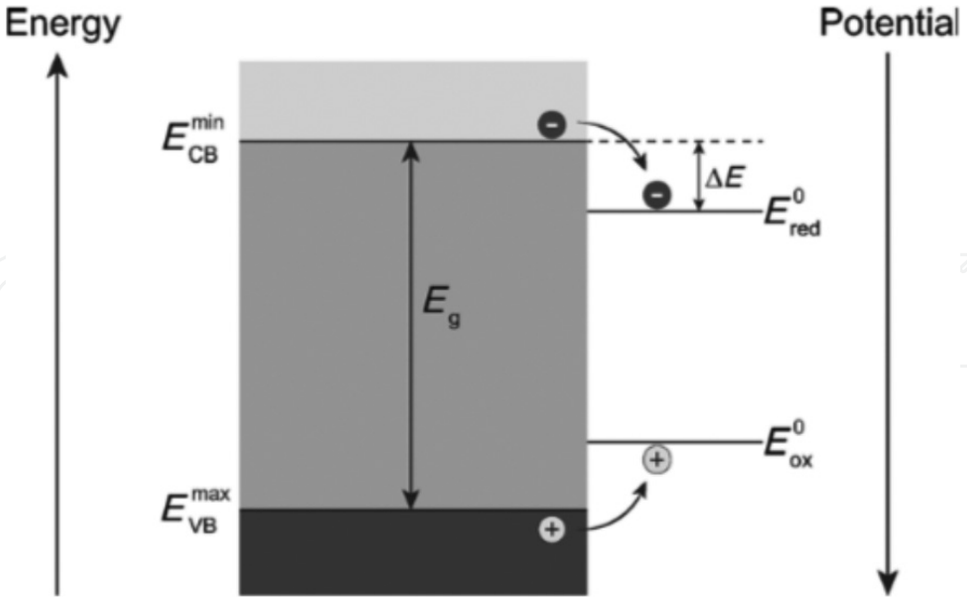

Figure 3. Thermodynamic constraints on the transfer of charge carriers to adsorbed molecules, and ΔE represents the kinetic overpotential of the reduction process. In this scheme, electrons and holes gain stability when moving down and up, respectively (reproduced from [43]).

http://dx.doi.org/10.5772/intechopen.74245

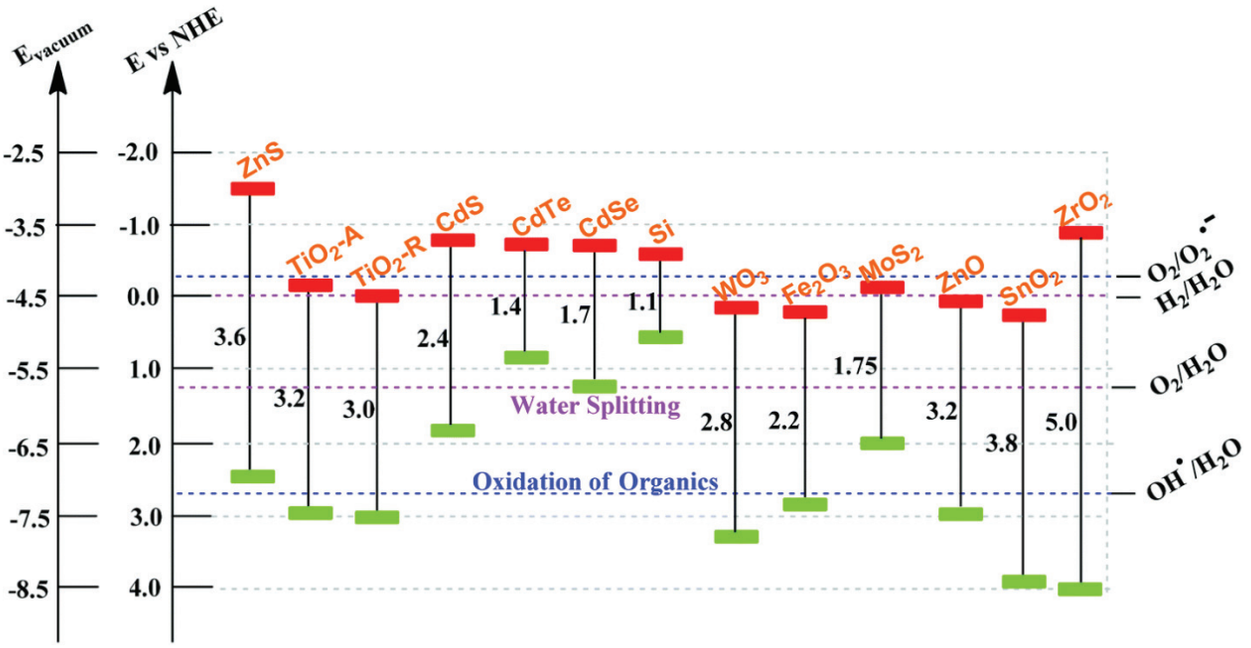

Figure 4. Bandgap energy structure of several common semiconductors on a potential scale (V) vs. NHE/vacuum (reproduced from [51]).

While choosing a photocatalyst for application in environmental remediation, it is also essential to take into account the reduction potentials (E) of the substrate, as well as those of the intermediates that are formed during the photocatalytic reaction(s). However, the reduction potentials for different organic or inorganic compounds are usually dependent on the reaction conditions such as pH and the employed electrolyte. The reduction potential of the couples $M/M^{\bullet -}$ refers to the reactions described by Eqs (7) and (8):

$$\text{oxidant} + e^- \rightarrow \text{Reductant} \tag{7}$$

$$\text{oxidant} + e^- + nH^+ \rightarrow \text{Reductant} \tag{8}$$

These reactions refer to one-electron reduction reactions—the potentials of which are given versus the standard hydrogen electrode (SHE). **Table 1** includes the reduction potentials of the most important inorganic species that may be present in photocatalytic systems.

For example, over a TiO_2 photocatalyst in pH 7 solution, reaction Eq. (9) is feasible because the redox potential of the $e_{cb}^- = -0.52$ V vs. SHE is sufficiently more negative than the reduction potential ($E^0(O_2/O_2^{\bullet -})$ = -0.28 V vs. SHE) of the superoxide radicals. Reaction (10) occurs because the redox potential of the $h_{vb}^+ = +2.53$ V vs. SHE is sufficiently more positive than the oxidation potential ($E^0(H_2O/OH^{\bullet}) = +2.27$ V vs. SHE) of the hydroxyl radical.

$$O_2 \text{ isonosorption}: \qquad O_2 + e_{cb}^- \rightarrow O_2^{\bullet -} \tag{9}$$

$$H_2O \text{ ionization}: \qquad H_{ads}^+ + OH_{ads}^- + h_{vb}^+ \rightarrow OH^{\bullet} + H^+ \tag{10}$$

Reductiom reaction	E^a, (V)	Remark
$aq + e^- \rightarrow e^-_{aq}$	−2.870	
$SO_4^{2-} + H_2O + e^- \rightarrow SO_3^{\bullet -} + 2OH^-$	−2.470	
$CO_2 + e^- \rightarrow CO_2^{\bullet -}$	−1.900	
$O_2 + e^- \rightarrow O_2^{\bullet -}$	−0.330	
$O_2 + H^+ + e^- \rightarrow HO_2^{\bullet -}$	−0.037	pH 0
$Cl_2 + e^- \rightarrow Cl_2^{\bullet -}$	0.420–0.600	
$I_2 + e^- \rightarrow I_2^{\bullet -}$	0.420–0.600	
$SO_3^{\bullet -} + e^- \rightarrow SO_3^{2-}$	0.630	pH >8
$Fe^{3+} + e^- \rightarrow Fe^{2+}$	0.570	
$HO_2^{\bullet} + e^- \rightarrow HO_2^-$	0.590	
$H_2O_2 + H^+ + e^- \rightarrow H_2O + HO^{\bullet}$	0.800	pH 7
$Ag^+ + e^- \rightarrow Ag$	0.800	
$NO_2^{\bullet} + e^- \rightarrow NO_2^-$	0.870–1.040	
$O_2^{\bullet -} + 2H^+ + e^- \rightarrow H_2O_2$	0.940	pH 7
$O_2^{\bullet -} + H^+ + e^- \rightarrow HO_2^-$	1.000	
$CO_3^{\bullet -} + H^+ + e^- \rightarrow HCO_3^-$	1.070	pH 7
$HS^{\bullet} + e^- \rightarrow HS^-$	1.150	
$O_3 + e^- \rightarrow O_3^{\bullet -}$	1.190–1.600	pH >11
$I^{\bullet} + e^- \rightarrow I^-$	1.270–1.420	
$HO_1^{\bullet} + H^+ + e^- \rightarrow H_2O_2$	1.420	pH 9
$CO_3^{\bullet -} + e^- \rightarrow CO_3^{2-}$	1.500	
$O_3 + H^+ + e^- \rightarrow HO_3^{\bullet}$	1.800	pH 7
$OH^{\bullet} + H^+ + e^- \rightarrow H_2O$	1.800–2.180	pH 7
$CN^- + e^- \rightarrow CN^-$	1.900	
$Br^- + e^- \rightarrow Br^-$	2.000	
$Cl^{\bullet} + e^- \rightarrow Cl^-$	2.200–2.600	
$Cl_2^{\bullet -} + e^- \rightarrow 2Cl^-$	2.300	
$NO_3^{\bullet} + e^- \rightarrow NO_3^-$	2.300–2.600	
$SO_4^{\bullet -} + e^- \rightarrow SO_4^{2-}$	2.430	
$OH^{\bullet} + H^+ + e^- \rightarrow H_2O$	2.590–2.850	pH 0
$F^{\bullet} + e^- \rightarrow F^-$	3.600	

[a]Reduction potential referring to one-electron reduction vs. SHE in the case of proton involvement, and *E* values may be used to estimate the standard potentials E^o as defined by the Nernst equation.

Table 1. Reduction potentials of some species that may be involved in photocatalytic systems (adapted from [51]).

Moreover, it is in fact critical to provide an overpotential for each process, to initiate and subsequently drive the electron transfer process. Without an overpotential, even a good photocatalyst cannot ensure sufficiently a high rate of reaction.

3. Beneficial roles of CQD materials in photocatalysis

3.1. Extends the optical absorption range of photocatalysts

The absorption of large portion of incident solar radiation by a photocatalyst is one of the key factors for achieving useful efficiencies in photocatalysis [52]. For wide bandgap semiconductors such as TiO_2, a common strategy for achieving this is through the use of photosensitizers. A photosensitizer is excited by low-energy photons to generate electrons that are subsequently injected into the conduction band of the wide bandgap photocatalyst. The common photosensitizers are usually characterized as expensive [53–55], toxic [56], unstable [57], and polluting [58]. These drawbacks limit the practical and large-scale application of conventional photosensitizers. Accordingly, it is essential to find an alternative photosensitizer material(s) that is free from these drawbacks and one that can harvest larger portion of the solar radiation. Carbon quantum dot appears to be such a material. It is easy to produce, cheap, nontoxic, green, stable, and abundant [1, 58, 59]. Additionally, it displays strong blue photoluminescence and good optical absorption in the UV and near-visible region [60]. Futhermore, CQDs exhibit upconversion photoluminescence properties [19, 61–63] and exhibit promising electron transfer properties [64, 65]. These optical characteristics of CQDs render them promising candidates as photosensitizers for photocatalytic applications. Three possible photsensitization mechanisms are proposed for CQDs in the literature. Firstly, CQD can be excited by a low-energy radiation to generate holes (h^+_{vb}) and electrons (e^-_{cb}). Under favorable thermodynamic condition, the photogenerated e^-_{cb} is injected into the conduction band of a wide bandgap photocatalyst (such as TiO_2) to initiate a reaction as shown in **Figure 5(a)** [19]. Secondly, the CQDs with upconversion PL properties can convert longer wavelength light to the short wavelength light, which in turn can excite a wide bandgap photocatalyst (ZnO) to form e^-_{cb}/h^+_{vb} pairs (**Figure 5(b)** [66]). Finally, addition of CQDs may lead to bandgap narrowing of the semiconductor owing to the chemical bonding between semiconductor and CQD, which results in the extended light absorption range as shown in **Figure 5(c)** [67].

Recently, several reports have been published that show CQDs to dramatically extend the optical absorption range of wide and narrow bandgap photocatalysts to the entire visible-light range and beyond [18–21, 58, 60, 62, 68–71]. For example, in a recent publication, Ye et al. [58] reported using CQDs to extend the light absorption range of $BiVO_4$ to the entire visible range. The resulting CQD/$BiVO_4$ composite photocatalyst achieved an absolute photocurrent density J_{abs} of 9.2 mA cm^{-2} as shown in **Figure 6(a)**. A photoanode fashioned from the composite (NiOOH/FeOOH/CQDs/$BiVO_4$) achieved a photocurrent density of 5.99 mA cm^{-2} at 1.23 V vs. RHE under AM 1.5G in KH_2PO_4 aqueous solution without a hole scavenger (pH 7) and record a high applied bias photon-to-current efficiency of 2.29% at 0.6 V vs. RHE. Ren et al. [18]

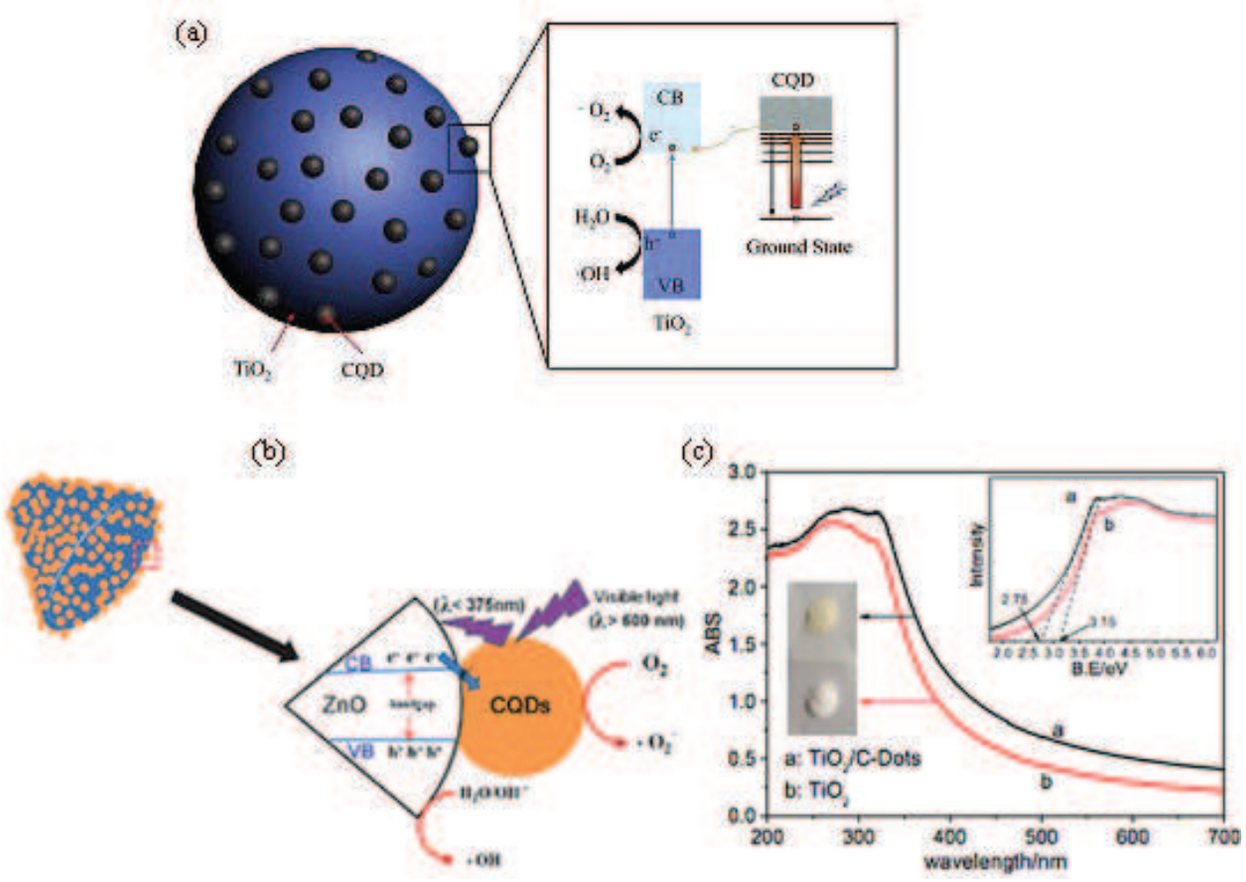

Figure 5. (a) Schematic illustration of the sensitization mechanism of CQDs based on (a) photoexcitation of CQDs [19], (b) upconversion photoluminescence [66], and (c) narrowing of band gap [67].

reported that coupling of CQDs with $MoSe_2$ resulted in a composite, CQD/$MoSe_2$ photocatalyst that is active over the entire range of the solar spectrum (**Figure 6(b)**).

Carbon quantum dots have also been applied as visible-light photosensitizer for non-noble metal H_2-evolution catalyst [24, 60, 68]. Martindale et al. used CQDs as a photosensitizer to energize a nickel-based molecular catalyst, Ni-bis-(diphosphine) (NiP) to produce H_2 under visible-light irradiation [24, 60]. A proposed scheme of H_2 production in the homogeneous CQD-NiP system is presented in **Figure 6(c)**. Irradiation of photoluminescent CQDs with visible-light results in the direct transfer of photoexcited electrons to the catalyst NiP with subsequent reduction of aqueous protons to H_2. The electron donor EDTA [60] or TCEP/EDTA [24] quenches the photogenerated holes in the CQDs. In a similar work, McCormick and coworkers [68] used a PVP-coated CQD as a photosensitizer for a nickel nanoparticle (NiNP) catalyst (**Figure 6(d)**) to produce H_2 at a much higher quantum yield of 6%. In this report, it was observed that the fluorescence quantum yield of CQDs increases with increasing PVP coating. However, H_2 production decreased when the PVP coating of CQD is greater than 20%. A total of 330 H_2/g CQD was collected from a 20% PVP-coated CDQ/Ni nanoparticle system at a pH of 4.51 after five irradiation with a 470-LED light source.

http://dx.doi.org/10.5772/intechopen.74245

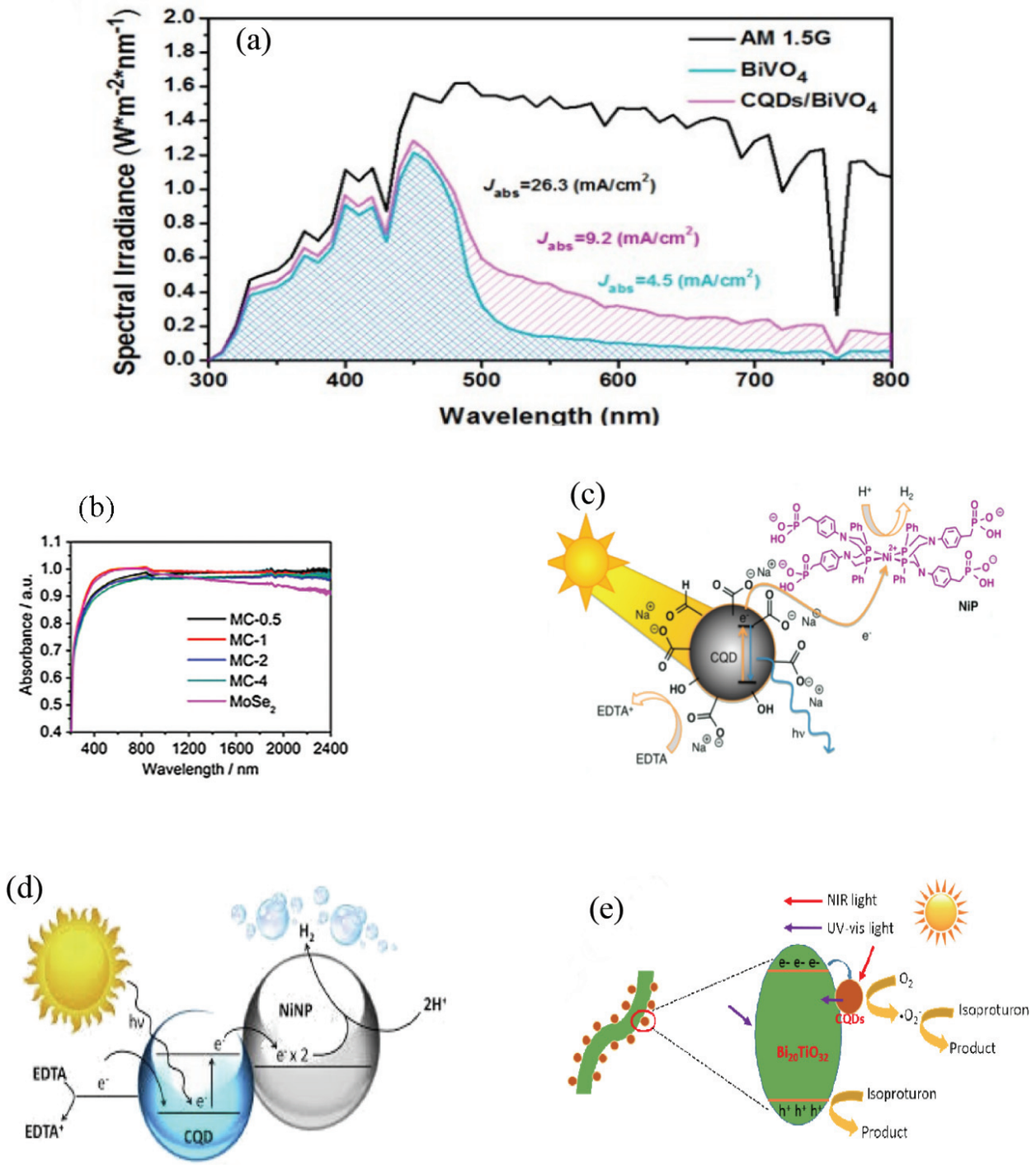

Figure 6. (a) Spectrum of the solar irradiance of AM 1.5G (ASTM G173-03) and the spectra showing the efficiencies of light absorption (LHE) of the $BiVO_4$ and CQDs/$BiVO_4$ photoanodes at 300–800 nm [58]. (b) Diffuse absorption spectra of $MoSe_2$ and the CQD/$MoSe_2$ (denoted as MC- in the plot) composites with different CQD contents [18]. Photosensitization of metal catalyst: (c) molecular NiP catalyst [60] and (d) nickel nanoparticle (NiNP) catalyst [68] under visible-light irradiation. (e) Sensitization of $Bi_{20}TiO_{32}$ by upconversion photoluminescence property of CQDs under NIR radiation [62].

Upconversion photoluminescence property (UCPL) of CQDs was used to improve the visible-light and NIR response of narrow bandgap composite photocatalysts. For example, Liu and coworkers [72] used the upconversion property of nitrogen-doped CQDs to improve the

visible-light and near infra-red response of graphitic carbon nitride (g-C_3N_4). Similarly, Mao et al. [62] improved the visible-light and NIR response of $Bi_{20}TiO_{32}$ by coupling it with CQDs. The resulting composite photocatalyst exhibited improved photoactivity under NIR irradiation. **Figure 6(e)** shows the proposed CQD sensitization mechanism.

3.2. Enhances charge separation and electron transfer

One of the main processes that limit the quantum efficiency of a photocatalytic system is the fast recombination of photogenerated charge carriers [40]. Therefore, to enhance the performance of a photocatalyst, it is essential to improve charge carrier separation and minimize the rate of their recombination. Several approaches have been devised to achieve this goal. These included strategies such as surface modification of the semiconductor particles with noble metals [73, 74], coupling of two semiconductor particles with different electronic levels [75–77], and using sacrificial reagents to scavenge for photogenerated electrons or holes [78–80]. Another strategy is to couple carbon-based materials with a photocatalyst because of their high charge storage capacity and electrical conductivity [81–83]. In particular, many reports have been recently published that show the beneficial effect of coupling of CQDs with photocatalysts [18–21, 63, 71, 84–86]. The intrinsic band gap and strong electron affinity [59, 65, 87] of CQDs give them the ability to readily accept photogenerated electrons from an electron donor such as a semiconductor with a more negative conduction band minimum. The transferred electrons are then shuttled freely along the conducting paths of the CQDs allowing for effective charge separation, stabilization, and prevention of charge recombination. The longer-lived charge carriers have greater probability to induce transformations, thus accounting for the much improved quantum efficiency of the CQD-based photocatalysts. **Figure 7** depicts a proposed photoinduced electron transfer mechanism on a layered composite of CQD/CdS photocatalyst [88].

Results of time-resolved (TR) PL and photocurrent measurements corroborated the slow recombination rates and enhanced the separation of electron-hole pairs observed in CQD-based photocatalysts. **Figure 7(b)** and **(d)** showed the time-resolved photoluminescence (TRPL) measurements on pure $Bi_{20}TiO_{32}$ and CdSe and their CQD-based counterparts with different amounts of CQD. Because the TRPL plots of the CQD composite photocatalysts exhibited lower PL intensities, it implies that the CQDs' modification effectively inhibits the recombination of photogenerated electron-hole-electron pairs in the hybrid photocatalysts. **Figure 7(c)** and **(e)** showed the corresponding photocurrent responses. The higher photocurrent signals recorded for the CQD-based photocatalysts compared to the pure photocatalysts demonstrated that much more photogenerated charge carriers were produced and the electron-hole pairs could separate more efficiently [62, 89].

3.3. Provides additional surface for adsorption and reaction

Another key role of CQD, which promotes photocatalytic activity, is its capacity to provide additional surface for adsorption and reaction of substrates. As a nanomaterial, CQDs possess a larger surface area to volume ratio, and thus, its composite with other nanomaterials potentially

http://dx.doi.org/10.5772/intechopen.74245

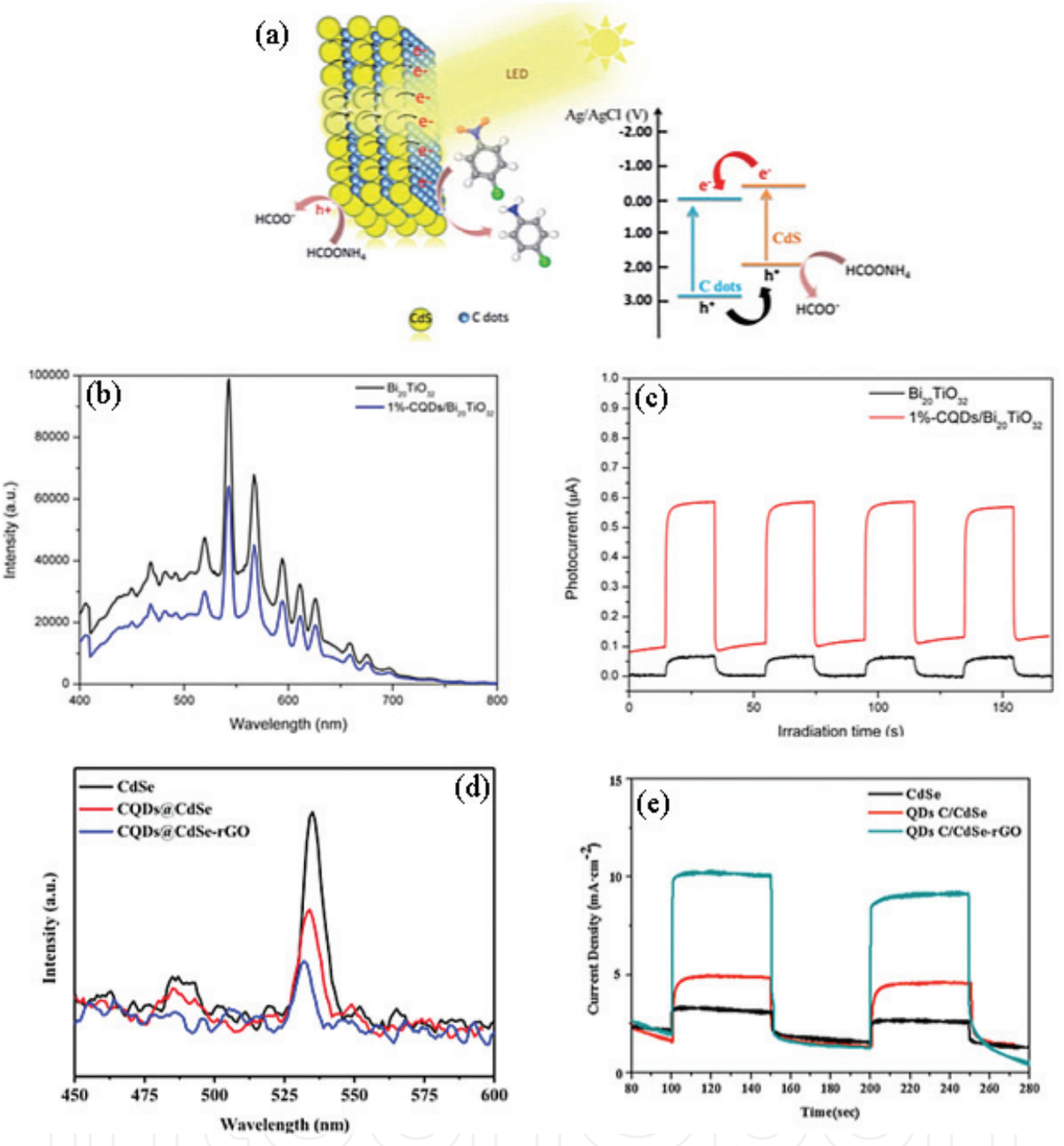

Figure 7. (a) Illustration of the mechanism of photoinduced electron transfer on a layered CQD/CdS nanocomposite photocatalyst from Ref. [88]. Plots (b)–(e) show the time-resolved photoluminescence and transient photocurrent profiles of pure photocatalysts and their CQD-based counterparts. Charts (b) and (c) for $Bi_{20}TiO_{32}$ and CQD/$Bi_{20}TiO_{32}$ from [62], and (d) and (e) pure for CdSe and CQD-based photocatalysts from Ref. [89].

acquires much enhanced surface area, thereby increasing the adsorption capacity. Like other carbon materials, adsorption capacity of CQD originates from the flexible sp^2-bonded carbon structure and the large surface area. Because the surface of CQDs contains a plethora of oxygenated functional groups [59], its adsorption capability depends on its interaction with the adsorbate. The aromatic regions of CQDs can form a π-π stacking interaction with organic adsorbates

containing aromatic structures to enhance their adsorption. On the other hand, the presence of functional groups such as carbonyl, epoxy, hydroxyl, and amino groups on the surface of CQDs promotes the adsorption of a wide variety of molecules and metal ions. The increased adsorption of target reactants on the surface of photocatalyst increases their chance of reacting with photogenerated reactive oxidative species, thus enhancing photocatalytic activity of the composite CQDs-based photocatalyst [90–92].

4. CQD-based semiconductor composites as visible-light active photocatalysts for water treatment

Recently, a large number of studies [17–21, 85, 86, 93–95] have reported on the application of CQD/semiconductor nanocomposites as photocatalysts for water purification owing to the exceptional properties exhibited by the composites. Carbon quantum dots have been coupled with variety of metal-oxide semiconductors such as TiO_2, Ag_3PO_4, SiO_2, $MoSe_2$, Bi_2MoO_6, and others and have found to be an excellent photocatalyst for the degradation of pollutants. **Table 2** summarizes some of the CQD-based composites that have been investigated as photocatalysts for the degradation of aqueous pollutants.

Chen et al. [17] reported the fabrication of nitrogen doped (i.e., NCQD/Ag_3PO_4) complex photocatalyst with improved activity under visible-light irradiation. As shown in **Figure 8(a)**, the activities of the hybrid NCQD/Ag_3PO_4 materials are significantly enhanced for the degradation of methyl orange (MO) compared with the pure Ag_3PO_4 under visible light (λ > 420 nm). A composite of NCQD/Ag_3PO_4 prepared from a 3 mL solution of 0.1 g CQD/L of distilled water denoted 3-NCQD/Ag_3PO_4 exhibited the highest activity. The 3-NCQD/Ag_3PO_4 sample eliminated 98% of the MO present in 18 min. In another report, Ren et al. [18] reported

CQD composite	Targeted pollutant	Visible-light source	Experiment conditions	η, %	Reference
CQD/Bi_2MoO_6	Methylene blue (MB)	300 W Xe lamp, ≤ 400-nm filter	100 mg cat., MB (100 mL, 10 mg/L), 30 C, 120 min	—	[20]
CQDs/Ag/Ag_2O	Methylene blue	250 W Xe lamp, ≤ 420-nm filter	50 mg cat., MB (100 mL, 10 mg/L), 150 min	≈ 100	[94]
CQD-TiO_2	Methylene blue	500 W Xe lamp, ≤ 420-nm filter	MB (15 mL, 5 mg/L), 100 min	35	[85]
CQD-TiO_2	Methylene blue	> 420 nm light	MB (50 mg/L), 25 min	≈ 100	[86]
CQD-TiO_2	Methylene blue	> 420 nm light	120 min	90	[19]
CQD-SiO_2	Methylene blue	> 420 nm light	MB (50 mg/L), 15 min	≈ 100	[86]
Fe_2O_3-CQD	Methylene blue	400 W halogen, ≤ 400-nm filter	50 mg cat., MB (100 mL, 20 mg/L), +35% H_2O_2, 90 min	97.3	[96]
Cu_2O-CQD	Methylene blue	400 W halogen, ≤ 400-nm filter	30 mg cat., MB (100 mL, 50 mg/L), 120 min	88	[97]

CQD composite	Targeted pollutant	Visible-light source	Experiment conditions	η, %	Reference
N-CQD	Methylene blue	> 420 nm light	10 μL cat., MB (3 mL, 1×10^{-4}mol dm^3),+$NaBH_4$, 6.5 min	≈ 100	[93]
Bi_2MoO_6-CDQ	Ciprofloxacin (CIP)	300 W Xe lamp with 400-nm filter	100 mg cat., CIP (100 mL, 10 mg/L), 30°C, 120 min	88	[20]
CDQ/Bi_2WO_6	Ciprofloxacin	300 W Xe lamp, ≤ 400-nm filter	50 mg cat., CIP (100 mL, 10 mg/L), 120 min	87	[21]
CQD/BiOBr	Ciprofloxacin	300 W Xe lamp, ≤ 400 nm filter	30 mg cat., CIP (100 mL, 10 mg/L), 4 h	44.3	[95]
Bi_2MoO_6-CDQ	Bisphenol A (BPA)	300 W Xe lamp, 400-nm filter	100 mg cat., BPA (100 mL, 10 mg/L), 30°C, 120 min	54	[20]
CQDs/BiOI	Bisphenol A	300 W Xe lamp, ≤ 420-nm filter	30 mg, 50 mg, 70 mg Cat., BPA (100 mL, 10 mg/L), 120 min	99	[84]
Bi_2WO_6-CDQ	Bisphenol A	300 W Xe lamp, ≤ 400-nm filter	50 mg cat., BPA (100 mL, 10 mg/L), 120 min	—	[21]
CQD/BiOBr	Bisphenol A	300 W Xe lamp, ≤ 400-nm filter	50 mg cat., BPA (100 mL, 10 mg/L),	66	[95]
Bi_2MoO_6 − CDQ	Tetracycline chloride (TC)	300 W Xe lamp, 400-nm filter	100 mg cat., TC (100 mL, 20 mg/L), 30, 120 min	—	[20]
CQDs/BiOI	Tetracycline chloride	300 W Xe lamp, ≤ 420-nm filter	30 mg, 50 mg, 70 mg Cat., TC (100 mL, 20 mg/L), 120 min	68	[84]
Bi_2WO_6 − CDQ	Tetracycline chloride	300 W Xe lamp, ≤ 400-nm filter	50 mg cat., TC (100 mL, 20 mg/L), 120 min	—	[21]
$MoSe_2$ − CDQ	Cr^6+	> 420 nm light	180 min	99	[18]
Ag_3PO_4 − CQD	Methyl orange (MO)	150 W Xe lamp, ≤ 420-nm filter	200 mg cat., MO (100 mL, 66 ppm), 25 min	≈ 100	[70]
CQD − TiO_2	Rhodamine B (RhB)	500 W Xe lamp, ≤ 420-nm filter	100 mg cat., MB (100 mL, 10 ppm), 60 min	95.4	[71]
CQDs/BiOI	Rhodamine B	300 W Xe lamp, ≤ 420-nm filter	30 mg, 50 mg, 70 mg Cat., RhB (100 mL, 10 mg/L), 30 min	61	[84]
CQD/BiOBr	Rhodamine B	300 W Xe lamp, ≤ 400-nm filter	20 mg cat., RhB (100 mL, 10 mg/L), 30 min	≈ 100	[95]
CQDs/Ag/Ag_2O	Rhodamine B	150 W NIR lamp, ≤ 700-nm filter	50 mg cat., RhB (100 mL, 10 mg/L), 150 min	48	[94]
Bi_2WO_6-CDQ	Rhodamine B	300 W Xe lamp, ≤ 400-nm filter	50 mg cat., RhB (100 mL, 10 mg/L), 120 min	—	[21]
CQDs/BiOI	Rhodamine B	300 W Xe lamp, ≤ 400-nm filter	30 mg cat., RhB (100 mL, 10 mg/L), 120 min	94.9	[98]
CQDs/CdS	Nitro-benzene	3 W LED light, ≤ 420-nm filter	30 mg cat., RhB (15 mL, 10 mg/L), 120 min, +$HCOONH_4$	—	[88]

Table 2. Different CQD-based composites used as photocatalysts used for water purification under visible-light irradiation.

improved activity for the reduction of Cr(VI) ion over CQD/$MoSe_2$ composite photocatalyst compared to the activity over pure $MoSe_2$ (**Figure 8(b)**). Similarly, Xie et al. also reported on the beneficial effects of complexing CQDs with $Bi_{20}TiO_{32}$ photocatalysts. Visible light active to improve the rate of charge transfer and reducing the rate of h^+_{vb}-e^-_{cb} recombination in $Bi_{20}TiO_{32}$ photocatalysts. The resulting CQD/$Bi_{20}TiO_{32}$ composites exhibited improved photocatalytic activities as shown in **Figure 8(c)**.

Li et al. [86] first reported the exploitation of the unique optical properties of CQDs in photocatalysis. The team synthesized TiO_2/CQDs and SiO_2/CQDs nanocomposite systems (**Figure 9a**) from CQDs with upconversion photoluminescence (PL) properties (**Figure 9b**) and used them to investigate the degradation of aqueous methylene blue (MB) under visible light. The as-synthesized CQDs-based photocatalysts exhibited enhanced ability to promote the degradation of the dye compared to their precursor components (CDQs, TiO_2, or SiO_2) as shown in **Figure 9c**. Under the given experimental conditions (50 mgL^{-1} MB solution, suspended TiO_2/CQDs or SiO_2/CQDs, 300 W halogen lamp irradiation) used, the MB was almost completely degraded in 15 and 25 min over SiO_2/CQDs and TiO_2/CQDs, respectively.

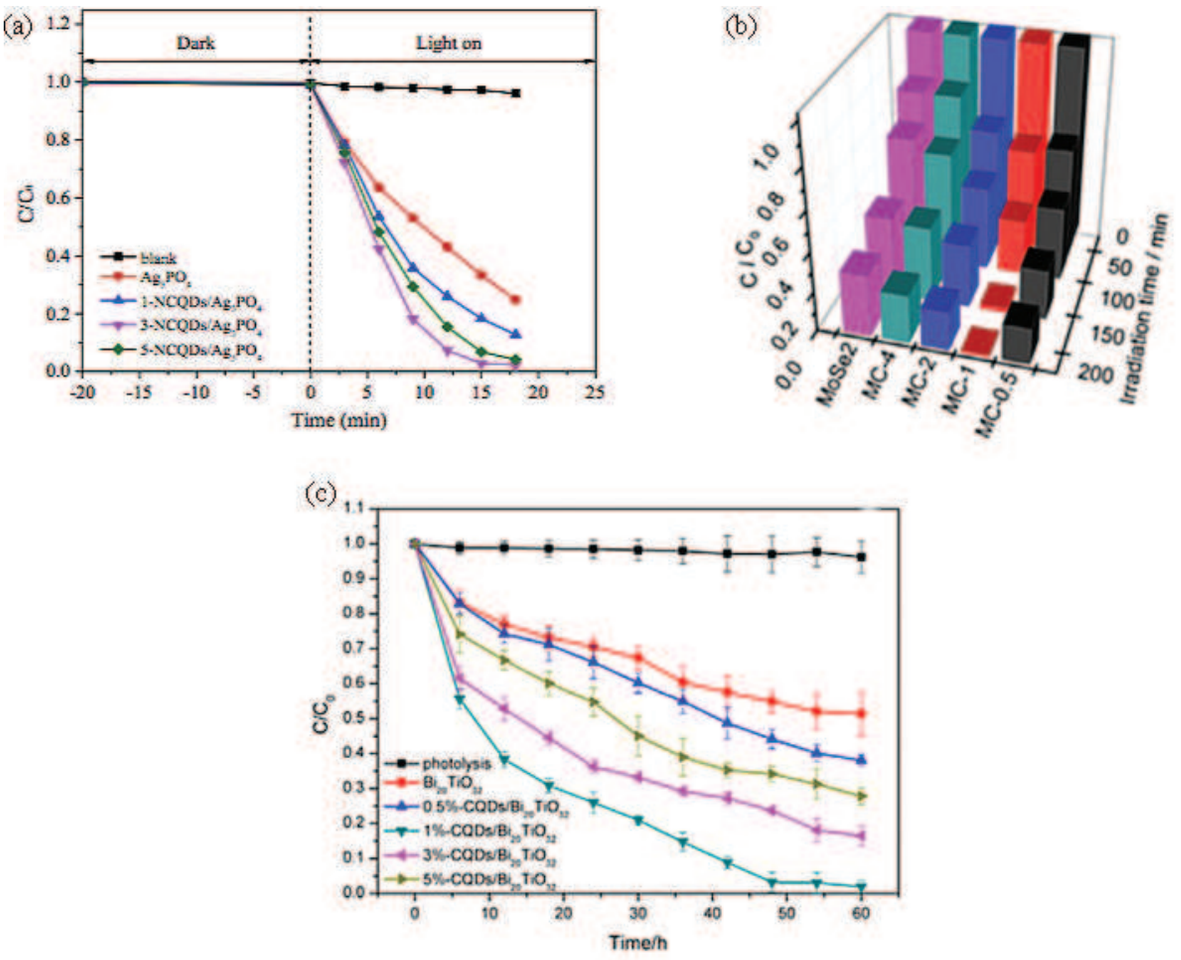

Figure 8. Photocatalytic performance of (a) MO over NCQD/Ag_3PO_4. (b) Cr(VI) over CQD/$MoSe_2$. (c) Isoproturon over CQD/$Bi_{20}TiO_{32}$.

Li and co-workers attributed the enhanced photocatalytic activities of the nanocomposites under visible light to upconversion and efficient charge carrier separation in the nanocomposite systems. The former allows CQDs to emit short-wavelength photons after absorbing visible light. The emitted short-wavelength UV light then induces photoexcitation of the TiO_2 and SiO_2 to generate the electron/hole (e^-_{cb}/h^+_{vb}) redox pairs that go to initiate the process of MB degradation via the generation reactive oxygen species such as $O_2^{\bullet -}$ and $OH^{\bullet}$ and others. The appropriate position of the conduction band edge of the CQDs allows electron transfer from the surface of the semiconductors, thereby enhancing charge carrier separation and inhibiting recombination resulting in the increased number of e^-_{cb} and h^+_{vb} available for photoreactions.

Yu et al. [96] reported the synthesis of CQDs/Fe_2O_3 complex photocatalysts via a facile solvent-thermal process in an aqueous solution (**Figure 10a**). The photocatalytic activity of photocatalyst was evaluated by the degradation of MB as a model contaminant under visible-light irradiation. The results (**Figure 10b**) showed that coupling of CQDs with Fe_2O_3 greatly enhances the

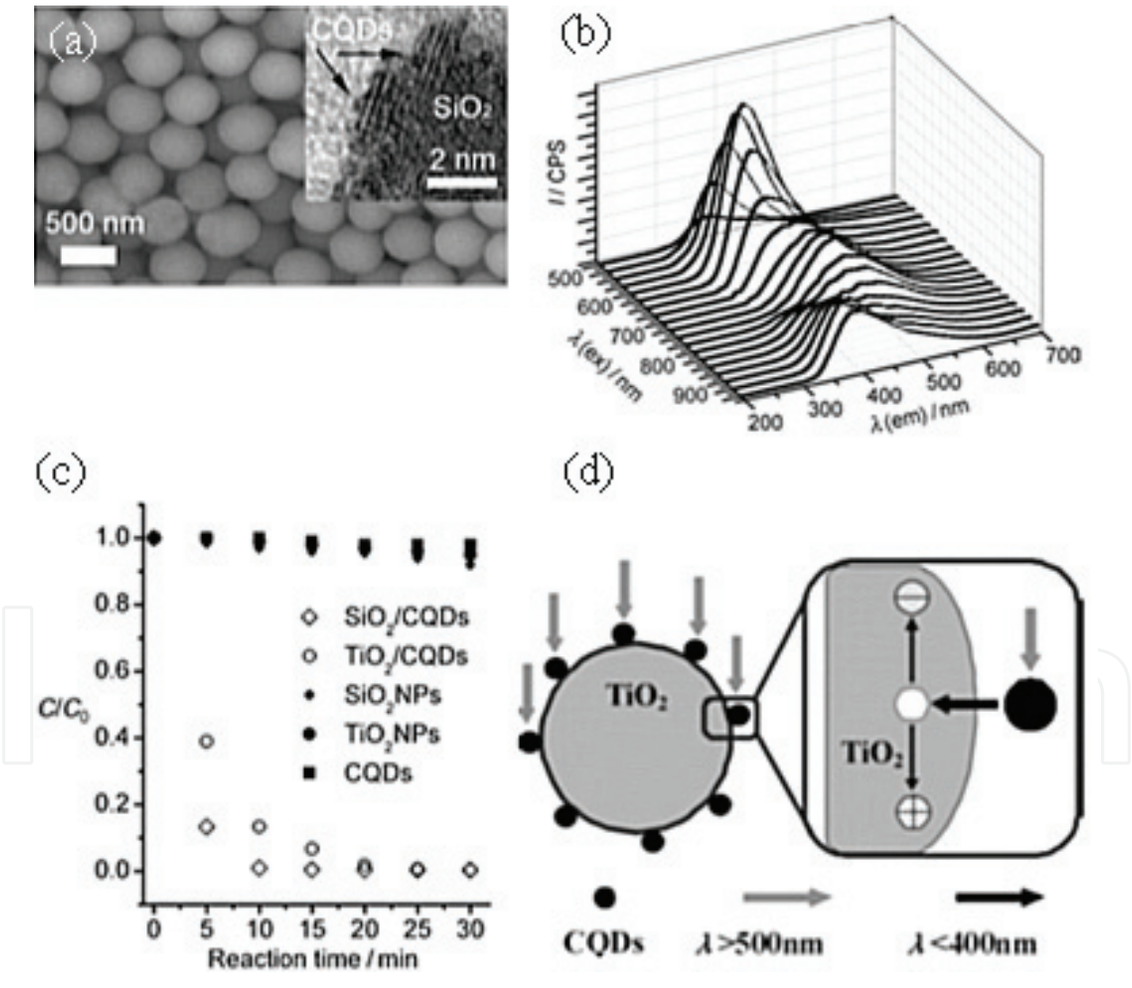

Figure 9. (a) A representative SEM image of the SiO_2/CQDs nanocomposite photocatalyst. Inset shows the corresponding HRTEM image. (b) Excitation-emission profile showing the upconversion PL property of the as-synthesized CQDs. (c) Degradation profile of MB in suspensions of different CQDs-based photocatalysts and control samples. (d) Scheme showing the postulated explanation of the mechanism of photocatalysis over CQDs-based photocatalyst. TiO_2/CQDs are used as a representative (reproduced from [86]).

decomposition of MB under visible-light irradiation. The authors attributed the enhanced activity of the photocatalyst to the mesoporous architecture and large surface area of the α-Fe_2O_3, which provides more abundant active sites for the adsorption and degradation of MB to occur and also for the effective electron transfer from the conduction band of the Fe_2O_3 particle to the conducting networks of the loaded CQDs as shown in **Figure 10c**.

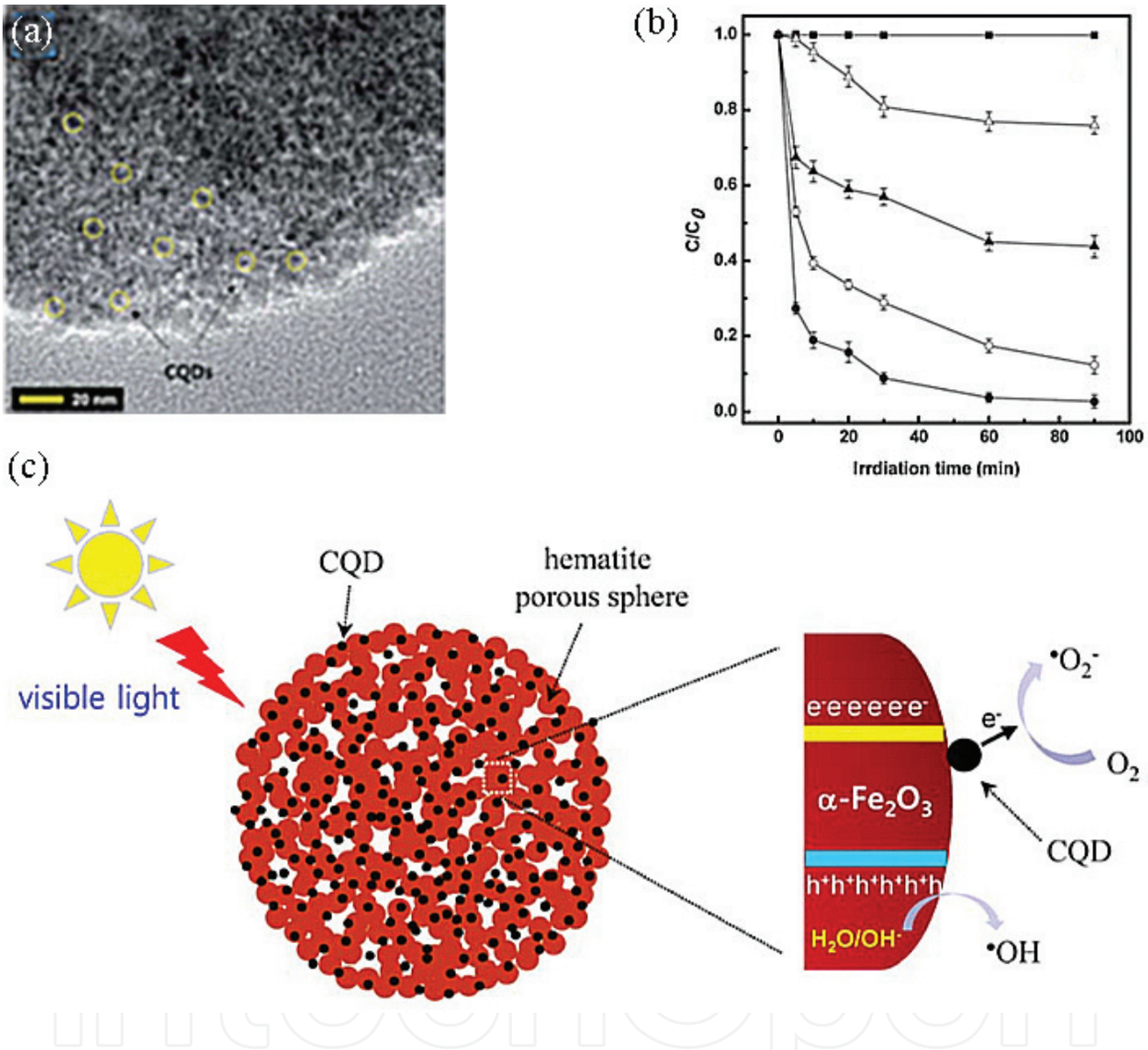

Figure 10. (a) HRTEM image of the CQDs/Fe_2O_3 photocatalysts. (b) Comparison of MB degradation profile in the presence of different catalysts: (■) CQD/Fe_2O_3 without light, (⊿)Fe_2O_3, (▲)$Fe_2O_3 + H_2O_2$, (○) CQD/Fe_2O_3, and (•) CQD/$Fe_2O_3 + H_2O_2$ (reproduced from [96]).

5. Conclusions and outlook

In summary, various types of carbon quantum dots/semiconductor composites have been investigated for the design of novel materials for water remediation via heterogenous photocatalysis. The coupling of CQDs with semiconductors synergistically enhances the activity of the photocatalysts for the degradation of various waterborne pollutants. The unique properties of CQDs, in conjunction with size-dependent properties of nanomaterials, induce

further functionalities to the composites such as high adsorption capacity, extended light absorption range, and improved charge separation properties along with high stability. Despite the confirmation of the excellent activity of CQDs-based photocatalystsic aforementioned reports, the applicability of the heterogeneous photocatalytic technology in large-scale water treatment is constrained by several key technical issues that have to be addressed.

The main constraints associated with the field scale application of CQD-based photocatalysts essentially lies in the design of (i) a catalyst that can utilize large portion of the solar spectra, (ii) catalyst immobilization strategy to provide a cost-effective solid-liquid separation, (iii) improvement in the photocatalytic operation for wider pH range and to minimize the addition of oxidant additives, (iv) new integrated or coupling system for enhanced photomineralization or photodisinfection kinetics, and (v) effective design of photocatalytic reactor system or parabolic solar collector for higher utilization of solar energy to reduce the electricity costs.

Acknowledgements

The authors gratefully acknowledge the financial support of the Tertiary Education Trust Fund of the Nigeria Ministry of Education.

Author details

Abdullahi Baba Makama[1]*, Muneer Umar[1] and Shettima Abdulkadir Saidu[2]

*Address all correspondence to: abmakama@hotmail.com

1 Department of Chemical Engineering Technology, The Federal Polytechnic, Nasarawa, Nigeria

2 Department of Science Laboratory Technology, The Federal Polytechnic, Nasarawa, Nigeria

References

[1] Baker SN, Baker GA. Luminescent carbon nanodots: emergent nanolights. Angewandte Chemie (International Ed. in English). 2010;**49**(38):6726-6744. DOI: 10.1002/anie.200906623. ISSN: 1521-3773 (Electronic); 1433-7851 (Linking)

[2] Yang P, Zhao J, Wang J, Cui H, Li L, Zhu Z. Multifunctional nitrogen-doped carbon nanodots for photoluminescence, sensor, and visible- light-induced H_2 production. ChemPhysChem. 2015;**16**(14):3058-3063. DOI: 10.1002/cphc.201500447. ISSN: 1439-7641 (Electronic); 1439-4235 (Linking)

[3] Yang P, Zhao J, Wang J, Cao B, Li L, Zhu Z. Construction of Z-scheme carbon nanodots/WO_3 with highly enhanced photocatalytic hydrogen production. Journal of Materials Chemistry A. 2015;**3**(16):8256-8259. DOI: 10.1039/C5TA00657K

[4] Liu J, Zhu W, Yu S, Yan X. Three dimensional carbogenic dots/TiO_2 nanoheterojunctions with enhanced visible light-driven photocatalytic activity. Carbon. 2014;**79**:369-379. DOI: 10.1016/j.carbon.2014.07.079. URL: http://www.sciencedirect.com/science/article/pii/S0008622314007301

[5] Wang H, Wei Z, Matsui H, Zhou S. Fe_3O_4/carbon quantum dots hybrid nanoflowers for highly active and recyclable visible-light driven photocatalyst. Journal of Materials Chemistry A. 2014;**2**(38):15740-15745. DOI: 10.1039/C4TA03130J

[6] Shen J, Li Y, Su Y, Zhu Y, Jiang H, Yang X, Li C. Photoluminescent carbon-nitrogen quantum dots as efficient electrocatalysts for oxygen reduction. Nanoscale. 2015;**7**(5): 2003-2008. DOI: 10.1039/c4nr06484d. ISSN: 2040-3372 (Electronic); 2040-3364 (Linking)

[7] Garg B, Bisht T. Carbon nanodots as peroxidase nanozymes for biosensing. Molecules. 2016;**21**(12). DOI: 10.3390/molecules21121653. ISSN: 1420-3049 (Electronic); 1420-3049 (Linking)

[8] Hao J, Wang L, Wang Y, Sun X, Zhang G, Dong S. Versatile self-assembly and biosensing applications of DNA and carbon quantum dots coordinated cerium ions. Chemistry. 2017. DOI: 10.1002/chem.201701709. ISSN: 1521-3765 (Electronic); 0947-6539 (Linking)

[9] Lan L, Yao Y, Ping J, Ying Y. Recent advances in nanomaterial-based biosensors for antibiotics detection. Biosensors and Bioelectronics. 2017;**91**:504-514. DOI: 10.1016/j.bios.2017.01.007. ISSN: 1873-4235 (Electronic); 0956-5663 (Linking)

[10] Liu Q, Ma C, Liu X-P, Wei Y-P, Mao C-J, Zhu J-J. A novel electrochemiluminescence biosensor for the detection of microRNAs based on a DNA functionalized nitrogen doped carbon quantum dots as signal enhancers. Biosensors and Bioelectronics. 2017;**92**:273-279. DOI: 10.1016/j.bios.2017.02.027. ISSN: 1873-4235 (Electronic); 0956-5663 (Linking)

[11] Baig MMF, Chen Y-C. Bright carbon dots as fluorescence sensing agents for bacteria and curcumin. Journal of Colloid and Interface Science. 2017;**501**:341-349. DOI: 10.1016/j.jcis.2017.04.045. ISSN: 1095-7103 (Electronic); 0021-9797 (Linking)

[12] Cheng C, Shi Y, Li M, Xing M, Wu Q. Carbon quantum dots from carbonized walnut shells: Structural evolution, fluorescence characteristics, and intracellular bioimaging. Materials Science and Engineering C: Materials for Biological Applications. 2017;**79**:473-480. DOI: 10.1016/j.msec.2017.05.094

[13] Guo J, Liu D, Filpponen I, Johansson L-S, Malho J-M, Quraishi S, Liebner F, Santos HA, Rojas OJ. Photoluminescent hybrids of cellulose nanocrystals and carbon quantum dots as cytocompatible probes for in vitro bioimaging. Biomacromolecules. 2017. DOI: 10.1021/acs.biomac.7b00306. ISSN: 1526-4602 (Electronic); 1525-7797 (Linking)

[14] Yang X, Yang W, Shen X, Chunyan S, Yang J, Piao M, Jia F, Gao G, Zhang L, Lin Q. One-step synthesis of photoluminescent carbon dots with excitation-independent emission for selective bioimaging and gene delivery. Journal of Colloid and Interface Science. 2017;**492**: 1-7. DOI: 10.1016/j.jcis.2016.12.057. ISSN: 1095-7103 (Electronic); 0021-9797 (Linking)

[15] Pan J, Zheng Z, Yang J, Wu Y, Lu F, Chen Y, Gao W. A novel and sensitive fluorescence sensor for glutathione detection by controlling the surface passivation degree of carbon quantum dots. Talanta. 2017;**166**:1-7. DOI: 10.1016/j.talanta.2017.01.033. ISSN: 1873-3573 (Electronic); 0039-9140 (Linking)

[16] Lee JJ, Yazan LS, Abdullah CAC. A review on current nanomaterials and their drug conjugate for targeted breast cancer treatment. International Journal of Nanomedicine. 2017;**12**:2373-2384. DOI: 10.2147/IJN.S127329. ISSN: 1178-2013 (Electronic); 1176-9114 (Linking)

[17] Chen Q, Wang Y, Wang Y, Zhang X, Duan D, Fan C. Nitrogen-doped carbon quantum dots/Ag_3PO_4 complex photocatalysts with enhanced visible light driven photocatalytic activity and stability. Journal of Colloid and Interface Science. 2017;**491**:238-245. DOI: 10.1016/j.jcis.2016.12.013. ISSN: 1095-7103 (Electronic); 0021-9797 (Linking)

[18] Ren Z, Liu X, Chu H, Yu H, Xu Y, Zheng W, Lei W, Chen P, Li J, Li C. Carbon quantum dots decorated $MoSe_2$ photocatalyst for Cr(VI) reduction in the UV-vis-NIR photon energy range. Journal of Colloid and Interface Science. 2017;**488**:190-195. DOI: 10.1016/j.jcis.2016.10.077. ISSN: 1095-7103 (Electronic); 0021-9797 (Linking)

[19] Ke J, Li X, Zhao Q, Liu B, Liu S, Wang S. Upconversion carbon quantum dots as visible light responsive component for efficient enhancement of photocatalytic performance. Journal of Colloid and Interface Science. 2017;**496**:425-433. DOI: 10.1016/j.jcis.2017.01.121. ISSN: 1095-7103 (Electronic); 0021-9797 (Linking)

[20] Di J, Xia J, Ji M, Li H, Xu H, Li H, Chen R. The synergistic role of carbon quantum dots for the improved photocatalytic performance of Bi_2MoO_6. Nanoscale. 2015;**7**(26): 11433-11443. ISSN: 2040-3372 (Electronic); 2040-3364 (Linking). DOI: 10.1039/c5nr01350j

[21] Di J, Xia J, Ge Y, Li H, Ji H, Xu H, Zhang Q, Li H, Li M. Novel visible-light-driven CQDs/Bi_2WO_6 hybrid materials with enhanced photocatalytic activity toward organic pollutants degradation and mechanism insight. Applied Catalysis. B, Environmental. 2015;**168**: 51-61. DOI: 10.1016/j.apcatb.2014.11.057. URL: http://www.sciencedirect.com/science/article/pii/S092633731400770X

[22] Liu X-Y, Chen H, Wang R, Shang Y, Zhang Q, Li W, Zhang G, Juan S, Dinh CT, Pelayo Garcia de Arquer F, Li J, Jiang J, Mi Q, Si R, Li X, Sun Y, Long Y-T, Tian H, Sargent EH, Ning Z. 0D-2D quantum dot: Metal dichalcogenide nanocomposite photocatalyst achieves efficient hydrogen generation. Advanced Materials. June 2017;**29**(22). ISSN: 1521-4095 (Electronic); 0935-9648 (Linking). DOI: 10.1002/adma.201605646

[23] Shi R, Li Z, Yu H, Lu S, Zhou C, Waterhouse GIN, Wu L-Z, Zhang T. Effect of nitrogen doping level on the performance of N-doped carbon quantum dot/TiO_2 composites for photocatalytic hydrogen evolution. ChemSusChem. 2017. DOI: 10.1002/cssc.201700943. ISSN: 1864-564X (Electronic); 1864-5631 (Linking)

[24] Martindale BCM, Joliat E, Bachmann C, Alberto R, Reisner E. Clean donor oxidation enhances the H_2 evolution activity of a carbon quantum dot-molecular catalyst photosystem. Angewandte Chemie (International Ed. in English). 2016;**55**(32):9402-9406. ISSN: 1521-3773 (Electronic); 1433-7851 (Linking). DOI: 10.1002/anie.201604355

[25] Xu X, Bao Z, Zhou G, Zeng H, Hu J. Enriching photoelectrons via three transition channels in amino-conjugated carbon quantum dots to boost photocatalytic hydrogen generation. ACS Applied Materials & Interfaces. 2016;**8(22)**:14118-14124. DOI: 10.1021/acsami.6b02961. ISSN: 1944-8252 (Electronic); 1944-8244 (Linking)

[26] Liu J, Yang L, Liu N, Han Y, Zhang X, Huang H, Lifshitz Y, Lee S-T, Zhong J, Kang Z. Metal-free efficient photocatalyst for stable visible water splitting via a two-electron pathway. Science. 2015;**347**(6225):970. URL: http://science.sciencemag.org/content/347/6225/970.abstract

[27] Li Q, Cui C, Meng H, Jiaguo Y. Visible-light photocatalytic hydrogen production activity of $ZnInS_4$ microspheres using carbon quantum dots and platinum as dual co-catalysts. Chemistry, an Asian Journal. 2014;**9**(7):1766-1770. DOI: 10.1002/asia.201402128. ISSN: 1861-471X (Electronic); 1861-471X (Linking)

[28] Shiral Fernando KA, Sahu S, Liu Y, Lewis WK, Guliants EA, Jafariyan A, Wang P, Bunker CE, Sun Y-P. Carbon quantum dots and applications in photocatalytic energy conversion. ACS Applied Materials & Interfaces. 2015;**7**(16):8363-8376. DOI: 10.1021/acsami.5b00448. ISSN: 1944-8252 (Electronic); 1944-8244 (Linking)

[29] Li H, Zhang X, MacFarlane DR. Carbon quantum dots/Cu_2O Heterostructures for solar-light-driven conversion of CO_2 to methanol. Advanced Energy Materials. 2015;**5**(5): 1401077-n/a). DOI: 10.1002/aenm.201401077

[30] Sahu S, Liu Y, Wang P, Bunker CE, Shiral Fernando KA, Lewis WK, Guliants EA, Yang F, Wang J, Sun Y-P. Visible-light photoconversion of carbon dioxide into organic acids in an aqueous solution of carbon dots. Langmuir. 2014;**30**(28):8631-8636. ISSN: 1520-5827 (Electronic); 0743-7463 (Linking). DOI: 10.1021/la5010209

[31] Kou J, Lu C, Wang J, Chen Y, Xu Z, Varma RS. Selectivity enhancement in heterogeneous photocatalytic transformations. Chemical Reviews. 2017;**117**(3):1445-1514. DOI: 10.1021/acs.chemrev.6b00396. ISSN: 1520-6890 (Electronic); 0009-2665 (Linking)

[32] Mosconi D, Mazzier D, Silvestrini S, Privitera A, Marega C, Franco L, Moretto A. Synthesis and photochemical applications of processable polymers enclosing photoluminescent carbon quantum dots. ACS Nano. 2015;**9**(4):4156-4164. DOI: 10.1021/acsnano.5b00319. ISSN: 1936-086X (Electronic); 1936-0851 (Linking)

[33] Tomita O, Ohtani B, Abe R. Highly selective phenol production from benzene on a platinum-loaded tungsten oxide photocatalyst with water and molecular oxygen: Selective oxidation of water by holes for generating hydroxyl radical as the predominant source of the hydroxyl group. Catalysis Science & Technology. 2014;**4**(11):3850-3860. DOI: 10.1039/C4CY00445K

[34] Yu H, Shi R, Zhao Y, Waterhouse GIN, Wu L-Z, Tung C-H, Zhang T. Smart utilization of carbon dots in semiconductor photocatalysis. Advanced Materials. 2016;**28**(43): 9454-9477. ISSN: 1521-4095 (Electronic); 0935-9648 (Linking). DOI: 10.1002/adma.201602581

[35] Gaya UI, Abdullah AH. Heterogeneous photocatalytic degradation of organic contaminants over titanium dioxide: A review of fundamentals, progress and problems. Journal of Photochemistry and Photobiology. 2008;**9**(1):1-12

[36] Konstantinou IK, Albanis TA. (TiO_2)-assisted photocatalytic degradation of azo dyes in aqueous solution: Kinetic and mechanistic investigations: A review. Applied Catalysis. B, Environmental. 2004;**49**(1):1-14

[37] Houas A, Lachheb H, Ksibi M, Elaloui E, Guillard C, Herrmann J-M. Photocatalytic degradation pathway of methylene blue in water. Applied Catalysis. B, Environmental. 2001;**31**(2):145-157

[38] Herrmann J-M. Heterogeneous photocatalysis: Fundamentals and applications to the removal of various types of aqueous pollutants. Catalysis Today. 1999;**53**(1):115-129. DOI: 10.1016/S0920-5861(99)00107-8 URL: http://www.sciencedirect.com/science/article/pii/S0920586199001078

[39] Anders, Hagfeldt, Michael, Graetzel. Light-induced redox reactions in nanocrystalline systems. Chemical Reviews. 1995;**95**(1):49-68. DOI: 10.1021/cr00033a003

[40] Hoffmann MR, Martin ST, Choi W, Bahnemann DW. Environmental applications of semiconductor photocatalysis. Chemical Reviews. 1995;**95**(1):69-96. DOI: 10.1021/cr00033a004

[41] Fox MA, Dulay MT. Heterogeneous photocatalysis. Chemical Reviews. 1993;**93**(1):341-357. DOI: 10.1021/cr00017a016

[42] Linsebigler AL, Guangquan L, Yates JT. Photocatalysis on TiO_2 surfaces: Principles, mechanisms, and selected results. Chemical Reviews. 1995;**95**(3):735-758. DOI: 10.1021/cr00035a013

[43] Habisreutinger SN, Schmidt-Mende L, Stolarczyk JK. Photocatalytic reduction of CO_2 on TiO_2 and other semiconductors. Angewandte Chemie (International Ed. in English). July 2013;**52**(29):7372-7408. DOI: 10.1002/anie.201207199. ISSN: 1521-3773 (Electronic); 1433-7851 (Linking)

[44] Zhou H, Yongquan Q, Zeid T, Duan X. Towards highly efficient photocatalysts using semiconductor nanoarchitectures. Energy & Environmental Science. 2012;**5**(5):6732-6743

[45] Ni M, Leung MKH, Leung DYC, Sumathy K. A review and recent developments in photocatalytic water-splitting using TiO_2 for hydrogen production. Renewable and Sustainable Energy Reviews. 2007;**11**(3):401-425. ISSN: 1364-0321

[46] Brown TE, Brown TL, LeMay HEH, Bursten BE, Murphy C, Woodward P. Chemistry: The Central Science. Vol. 13, illustrated. Pearson; 2015. ISBN: 9780321910417. URL: https://books.google.com.ng/books?id=fhzpngEACAAJ

[47] Kisch H. Semiconductor photocatalysis—Mechanistic and synthetic aspects. Angewandte Chemie (International Ed. in English). 2013;**52**(3):812-847. DOI: 10.1002/anie.201201200

[48] Hakki A, Schneider J, Bahnemann D. Understanding the Chemistry of Photocatalytic Processes. Photocatalysis: Fundamentals and Perspectives. The Royal Society of Chemistry; 2016. Chapter 2. pp. 29-50. ISBN: 978-1-78262-041-9. DOI: 10.1039/9781782622338-00029

[49] Ohtani B. Revisiting the fundamental physical chemistry in heterogeneous photocatalysis: Its thermodynamics and kinetics. Physical Chemistry Chemical Physics. 2014;**16**(5):1788-1797. DOI: 10.1039/C3CP53653J

[50] Herrmann J-M, Guillard C, Pichat P. Heterogeneous photocatalysis: An emerging technology for water treatment. Catalysis Today. 1993;**17**(1–2):7-20

[51] Wu W, Jiang C, Roy VAL. Recent progress in magnetic iron oxide-semiconductor composite nanomaterials as promising photocatalysts. Nanoscale. 2015;**7**(1):38-58. DOI: 10.1039/C4NR04244A

[52] Rothenberger G, Comte P, Grätzel M. A contribution to the optical design of dye-sensitized nanocrystalline solar cells. Solar Energy Materials & Solar Cells. 1999;**58**(3):321-336. DOI: 10.1016/S0927-0248(99)00015-X. URL: http://www.sciencedirect.com/science/article/pii/S092702489900015X

[53] Maeda K, Sahara G, Eguchi M, Ishitani O. Hybrids of a ruthenium(II) polypyridyl complex and a metal oxide nanosheet for dye-sensitized hydrogen evolution with visible light: Effects of the energy structure on photocatalytic activity. ACS Catalysis. 2015;**5**(3):1700-1707. DOI: 10.1021/acscatal.5b00040

[54] Ozawa H, Honda S, Katano D, Sugiura T, Arakawa H. Novel ruthenium sensitizers with a dianionic tridentate ligand for dye-sensitized solar cells: The relationship between the solar cell performances and the electron-withdrawing ability of substituents on the ligand. Dalton Transactions. 2014;**43**:8026-8036. DOI: 10.1039/C3DT52873A

[55] Ardo S, Meyer GJ. Photodriven heterogeneous charge transfer with transition-metal compounds anchored to TiO_2 semiconductor surfaces. Chemical Society Reviews. 2009;**38**:115-164. DOI: 10.1039/B804321N

[56] Zhang X, Yu L, Wu J, Jing J, Fang B. Improved performance of CdSe/CdS/PbS co-sensitized solar cell with double-layered TiO_2 films as photoanode. Optics Communication. 2017;**395**:117-121. DOI: 10.1016/J.OPTCOM.2016.05.026. URL: http://www.sciencedirect.com/science/article/pii/S0030401816303789

[57] Sakai T, Mersch D, Reisner E. Photocatalytic hydrogen evolution with a hydrogenase in a mediator-free system under high levels of oxygen. Angewandte Chemie, International Edition. 2013;**52**(47):12313-12316. DOI: 10.1002/anie.201306214

[58] Ye K-H, Wang Z, Jiuwang G, Xiao S, Yuan Y, Zhu Y, Zhang Y, Mai W, Yang S. Carbon quantum dots as a visible light sensitizer to significantly increase the solar water splitting

performance of bismuth vanadate photoanodes. Energy & Environmental Science. 2017; **10**(3):772-779. DOI: 10.1039/C6EE03442J

[59] Lim SY, Shen W, Gao Z. Carbon quantum dots and their applications. Chemical Society Reviews. 2015;**44**(1):362-381

[60] Martindale BCM, Hutton GAM, Caputo CA, Reisner E. Solar hydrogen production using carbon quantum dots and a molecular nickel catalyst. Journal of the American Chemical Society. 2015;**137**(18):6018-6025. DOI: 10.1021/jacs.5b01650

[61] Jin Q, Gubu A, Chen X, Tang X. A photochemical avenue to photoluminescent N-dots and their upconversion cell imaging. Scientific Reports. 2017;**7**(1):1793. DOI: 10.1038/s41598-017-01663-x

[62] Xie R, Zhang L, Xu H, Zhong Y, Sui X, Mao Z. Construction of up-converting fluorescent carbon quantum dots/Bi_2OTiO_3 2 composites with enhanced photocatalytic properties under visible light. Chemical Engineering Journal. 2017;**310**(Part 1):79-90. DOI: 10.1016/j.cej.2016.10.089. URL: http://www.sciencedirect.com/science/article/pii/S1385894716314991

[63] Zhang X, Huang H, Liu J, Yang L, Kang Z. Carbon quantum dots serving as spectral converters through broadband upconversion of near-infrared photons for photoelectrochemical hydrogen generation. Journal of Materials Chemistry A. 2013;**1**(38):11529-11533. DOI: 10.1039/C3TA12568H

[64] Wang R, Lu K-Q, Tang Z-R, Yi-Jun X. Recent progress in carbon quantum dots: Synthesis, properties and applications in photocatalysis. Journal of Materials Chemistry C. 2017; **5**(8):3717-3734. DOI: 10.1039/C6TA08660H

[65] Wang X, Cao L, Lu F, Meziani MJ, Li H, Qi G, Zhou B, Harruff BA, Kermarrec F, Sun Y-P. Photoinduced electron transfers with carbon dots. Chemical Communications (Camb). 2009;**25**:3774-3776. DOI: 10.1039/B906252A. URL: http://www.ncbi.nlm.nih.gov/pmc/articles/PMC2767382/

[66] Yu H, Zhang H, Huang H, Yang L, Li H, Ming H, Kang Z. ZnO/carbon quantum dots nanocomposites: One-step fabrication and superior photocatalytic ability for toxic gas degradation under visible light at room temperature. New Journal of Chemistry. 2012; **36**(4):1031-1035

[67] Chen P, Wang F, Chen Z-F, Zhang Q, Yuehan S, Shen L, Yao K, Yang L, Cai Z, Lv W, Liu G. Study on the photocatalytic mechanism and detoxicity of gemfibrozil by a sunlight-driven TiO_2/carbon dots photocatalyst: The significant roles of reactive oxygen species. Applied Catalysis. B, Environmental. 2017;**204**(Supplement C):250-259. DOI: 10.1016/j.apcatb.2016.11.040. URL: http://www.sciencedirect.com/science/article/pii/S0926337316309079

[68] Virca CN, Winter HM, Goforth AM, Mackiewicz MR, McCormick TM. Photocatalytic water reduction using a polymer coated carbon quantum dot sensitizer and a nickel nanoparticle catalyst. Nanotechnology. 2017;**28**(19):195402. URL: http://stacks.iop.org/0957-4484/28/i=19/a=195402

[69] Prasannan A, Imae T. One-pot synthesis of fluorescent carbon dots from orange waste peels. Industrial and Engineering Chemistry Research. 2013;**52**(44):15673-15678

[70] Zhang H, Huang H, Ming H, Li H, Zhang L, Yang L, Kang Z. Carbon quantum dots/Ag_3PO_4 complex photocatalysts with enhanced photocatalytic activity and stability under visible light. Journal of Materials Chemistry. 2012;**22**(21):10501-10506

[71] Yu X, Liu J, Yu Y, Zuo S, Li B. Preparation and visible light photocatalytic activity of carbon quantum dots/TiO_2 nanosheet composites. Carbon. 2014;**68**:718-724

[72] Wang F, Chen P, Feng Y, Xie Z, Yang L, Yuehan S, Zhang Q, Wang Y, Yao K, Lv W, Liu G. Facile synthesis of N-doped carbon dots/g-C_3N_4 photocatalyst with enhanced visible-light photocatalytic activity for the degradation of indomethacin. Applied Catalysis. B, Environmental. 2017;**207**(Supplement C):103-113. DOI: 10.1016/j.apcatb.2017.02.024. URL: http://www.sciencedirect.com/science/article/pii/S0926337317301285

[73] Boxi SS, Paria S. Visible light induced enhanced photocatalytic degradation of organic pollutants in aqueous media using Ag doped hollow TiO_2 nanospheres. RSC Advances. 2015;**5**(47):37657-37668

[74] Nakajima A, Kobayashi T, Isobe T, Matsushita S. Preparation and visible-light photocatalytic activity of Au-supported porous CeO_2 spherical particles using templating. Materials Letters. 2011;**65**(19):3051-3054. DOI: 10.1016/j.matlet.2011.06.051. URL: http://www.sciencedirect.com/science/article/pii/S0167577X1100694X

[75] Xiong D, Chang H, Zhang Q, Tian S, Liu B, Zhao X. Preparation and characterization of $CuCrO_2$/TiO_2 heterostructure photocatalyst with enhanced photocatalytic activity. Applied Surface Science. 2015;**347**:747-754

[76] Xiong X, Chen H, Yiming X. Improved photocatalytic activity of TiO_2 on the addition of $CuWO_4$. Journal of Physical Chemistry C. Mar. 2015;**119**(11):5946-5953. DOI: 10.1021/jp510974f

[77] Wang W, Wang J, Wang Z, Wei X, Liu L, Ren Q, Gao W, Liang Y, Shi H. p-n junction CuO/$BiVO_4$ heterogeneous nanostructures: Synthesis and highly efficient visible-light photocatalytic performance. Dalton Transactions. 2014;**43**(18):6735-6743

[78] Wang M, Shen S, Li L, Tang Z, Yang J. Effects of sacrificial reagents on photocatalytic hydrogen evolution over different photocatalysts. Journal of Materials Science. May 2017; **52**(9):5155-5164. ISSN: 1573-4803. DOI: 10.1007/s10853-017-0752-z

[79] Li X, Low J, Jiaguo Y. Photocatalytic hydrogen generation. Photocatalysis: Applications. In: Dionysiou DD, Puma GL, JinhuaYe JS, Bahnemann D, editors. Energy and Environment Series. The Royal Society of Chemistry; 2016. Chapter 10. pp. 255-302. ISBN: 978-1-78262-709-8. DOI: 10.1039/9781782627104-00255

[80] Park H, Kim H-i, Moon G-h, Choi W. Photoinduced charge transfer processes in solar photocatalysis based on modified TiO_2. Energy & Environmental Science. 2016;**9**(2):411-433. DOI: 10.1039/C5EE02575C

[81] Xiang Q, Cheng B, Jiaguo Y. Graphene-based Photocatalysts for solar-fuel generation. Angewandte Chemie, International Edition. 2015;**54**(39):11350-11366

[82] Rawalekar S, Mokari T. Rational design of hybrid nanostructures for advanced photocatalysis. Advanced Energy Materials. 2013;**3**(1):12-27. DOI: 10.1002/aenm.201200511

[83] Zhang L-W, Hong-Bo F, Zhu Y-F. Efficient TiO_2 photocatalysts from surface hybridization of TiO_2 particles with graphite-like carbon. Advanced Functional Materials. 2008;**18**(15): 2180-2189. DOI: 10.1002/adfm.200701478

[84] Di J, Xia J, Ji M, Wang B, Yin S, Xu H, Chen Z, Li H. Carbon quantum dots induced ultrasmall BiOI nanosheets with assembled hollow structures for broad spectrum photocatalytic activity and mechanism insight. Langmuir. 2016;**32**(8):2075-2084. DOI: 10.1021/acs.langmuir.5b04308

[85] Sun M, Ma X, Chen X, Sun Y, Cui X, Lin Y. A nanocomposite of carbon quantum dots and TiO_2 nanotube arrays: Enhancing photoelectrochemical and photocatalytic properties. RSC Advances. 2014;**4**(3):1120-1127

[86] Li H, He X, Kang Z, Huang H, Yang L, Liu J, Lian S, Tsang CHA, Yang X, Lee S-T. Water-soluble fluorescent carbon quantum dots and photocatalyst design. Angewandte Chemie, International Edition. 2010;**49**(26):4430-4434

[87] Li J, Ma Y, Ye Z, Zhou M, Wang H, Ma C, Wang D, Huo P, Yan Y. Fast electron transfer and enhanced visible light photocatalytic activity using multi-dimensional components of carbon quantum dots @ 3D daisy-like In_2S_3/single-wall carbon nanotubes. Applied Catalysis. B, Environmental. 2017;**204**:224-238. DOI: 10.1016/j.apcatb.2016.11.021. URL: http://www.sciencedirect.com/science/article/pii/S0926337316308797

[88] Chai N-N, Wang H-X, Hu C-X, Wang Q, Zhang H-L. Wellcontrolled layer-by-layer assembly of carbon dot/CdS heterojunctions for efficient visiblelight- driven photocatalysis. Journal of Materials Chemistry A. 2015;**3**(32):16613-16620. DOI: 10.1039/C5TA03649F

[89] Huo P, Guan J, Zhou M, Ma C, Liu X, Yan Y, Yuan S. Carbon quantum dots modified CdSe loaded reduced graphene oxide for enhancing photocatalytic activity. Journal of Industrial and Engineering Chemistry. 2017;**50**:147-154. DOI: 10.1016/j.jiec.2017.02.008. URL: http://www.sciencedirect.com/science/article/pii/S1226086X17300709

[90] Makama AB, Salmiaton A, Saion EB, Choong TSY, Abdullah N. Microwave-assisted synthesis of porous ZnO/SnS_2 heterojunction and its enhanced photoactivity for water purification. Journal of Nanomaterials. 2015;**2015**:13. DOI: 10.1155/2015/108297

[91] Xie X, Kretschmer K, Wang G. Advances in graphene-based semiconductor photocatalysts for solar energy conversion: Fundamentals and materials engineering. Nanoscale. 2015; **7**(32):13278-13292. DOI: 10.1039/C5NR03338A

[92] Han C, Yang M-Q, Weng B, Yi-Jun X. Improving the photocatalytic activity and anti-photocorrosion of semiconductor ZnO by coupling with versatile carbon. Physical Chemistry Chemical Physics. 2014;**16**(32):16891-16903. DOI: 10.1039/C4CP02189D

[93] Arul V, Edison TNJI, Lee YR, Sethuraman MG. Biological and catalytic applications of green synthesized fluorescent N-doped carbon dots using *Hylocereus undatus*. Journal of Photochemistry and Photobiology B. 2017;**168**:142-148. DOI: 10.1016/j.jphotobiol.2017.02.007

[94] Chen J, Che H, Huang K, Liu C, Shi W. Fabrication of a ternary plasmonic photocatalyst CQDs/Ag/Ag_2O to harness charge flow for photocatalytic elimination of pollutants. Applied Catalysis B. 2016;**192**:134-144. DOI: 10.1016/j.apcatb.2016.03.056. URL: http://www.sciencedirect.com/science/article/pii/S0926337316302387

[95] Xia J, Di J, Li H, Xu H, Li H, Guo S. Ionic liquid-induced strategy for carbon quantum dots/BiOX (X = Br, Cl) hybrid nanosheets with superior visible light-driven photocatalysis. Applied Catalysis. B, Environmental. 2016;**181**:260-269. DOI: 10.1016/j.apcatb.2015.07.035. URL: http://www.sciencedirect.com/science/article/pii/S0926337315300540

[96] Byong Yong Yu And Seung-Yeop Kwak. Carbon quantum dots embedded with mesoporous hematite nanospheres as efficient visible light-active photocatalysts. Journal of Materials Chemistry 2012;**22**(17):8345-8353

[97] Li H, Liu R, Yang L, Huang H, Yu H, Ming H, Lian S, Lee S-T, Kang Z. Carbon quantum dots/Cu_2O composites with protruding nanostructures and their highly efficient (near) infrared photocatalytic behavior. Journal of Materials Chemistry. 2012;**22**(34):17470-17475

[98] Di J, Xia J, Ji M, Xu L, Yin S, Zhang Q, Chen Z, Li H. Carbon quantum dots in situ coupling to bismuth oxyiodide via reactable ionic liquid with enhanced photocatalytic molecular oxygen activation performance. Carbon. 2016;**98**(Supplement C):613-623. DOI: 10.1016/j.carbon.2015.11.015. URL: http://www.sciencedirect.com/science/article/pii/S0008622315304243